Comparison of Geometric Optics and Diffraction Effects in Radar Scattering From Steep and Breaking Waves

V. U. Zavorotny and A. G. Voronovich
NOAA/Earth System Research Laboratory
325 Broadway
Boulder, CO 80305-3328

***Abstract*—To address the issue of radar scattering from steep and breaking ocean waves, we developed an efficient and fast 2-D numerical full-wave approach to model both wave evolution and radar scattering from these waves. It enabled us to reproduce the main features of the temporal and polarization behavior of the radar signal such as sea spikes. In addition, to better understand the contribution of multiple scattering that might emerge from radar scattering on steep and breaking waves, we have modeled scattering using a ray-tracing approach that not only provides the ray picture but also supplies both the ray amplitude and the ray phase. This approach eliminates diffraction effects from consideration, leaving only geometric optics effects that include multiple reflections. As a result, angular dependencies of the scattering cross section based on the ray approach were calculated and compared with corresponding values from the full-wave approach. Generally, better agreement between these two approaches is obtained for forward scattering directions than for backscattering directions. Ray simulation for a backscattering direction does not reproduce the HH/VV ratio with the spikes observed in the full-wave solution. This indicates that diffraction effects are critical for explaining important features of backscattering from breaking waves. The role of multiple reflections from the breaking wave profile in creating spikes with an anomalous HH/VV ratio proved to be negligible.**

I. Introduction

Numerical modeling of wave breaking and the subsequent modeling of full-wave electromagnetic (EM) scattering poses a significant challenge in terms of the complexity of codes and computational time. However, this is the only alternative when the problem cannot be handled using analytical methods [1]. Several methodologies based on direct numerical simulations have been proposed in the literature (see, e.g. [2, 3]). Recently, we employed a fast and efficient numerical approach equally convenient for use when dealing both with hydrodynamic and EM parts of the 2-D radar scattering problem [4, 5]. Using this approach we successfully reproduced the main features of temporal and polarization behavior for a scattering cross section from breaking waves and related Doppler spectra that are similar to those observed in experiments [6, 7].

Although numerical modeling of scattering is an efficient way for calculating a cross section when analytical approaches are not available, it leaves open the question of what specific physical mechanism is responsible for a particular feature of the scattered signal (e.g., sea spikes). To shed some light on the peculiarities of multiple scattering that might emerge from radar scattering on steep and breaking waves, we have undertaken numerical modeling of the same process, applying a ray-tracing approach to the problem. Generally, this would eliminate all kinds of diffraction effects from consideration, leaving only geometric optics effects that also include multiple reflections, (such as a "whispering gallery" effect), and interference between different rays.

II. Modeling of breaking waves

To model time-dependent surface profiles of a breaking gravity wave that can be non-single-valued in (x,z) Cartesian coordinates, a 2-D code has been developed that is based on the kinematic boundary condition and the Bernoulli equation in the Lagrangian form. If a parametrically defined surface profile $x(t,s)$, $z(t,s)$, and the potential of fluid particles $\varphi(t,s)$ are known at a certain moment in time, one can solve the Dirichlet boundary problem and calculate the Dirichlet-to-Neumann (DtN) linear operator which maps the value of the surface potential $\varphi(t,s)$ onto the normal derivative of the potential, $\partial\varphi/\partial\vec{n}$, at the surface points. Since the potential φ along the surface is known, the gradient of the potential (i.e., the velocity vector) at the surface points is calculated using the DtN operator. Those values are used in both kinematic boundary conditions and the Bernoulli equation for finding the surface profile and values of the surface potential at the next moment of time. Time-marching in numerical simulations is accomplished according to the Runge-Kutta scheme. More details about the hydrodynamic code and its performance can be found in [4, 5].

To simulate the evolution of the breaking wave profiles, we use the superposition of two moderately stable Stokes

waves of 1 m length as an initial condition. The resulting wave moves into a breaking phase when the crests of these two initial waves propagating at different speeds overlap. Subsequently, the wave profile loses smoothness, and the program stops. This process is illustrated in Figure 1, which represents some of the 180 wave profiles obtained for every 0.003 s used later in radar scattering simulations. For example, it was observed that at $t = 0.45$ *s* (profile #150), the front face of the wave becomes almost vertical, and then the wave breaks (see profiles from #168 to #180).

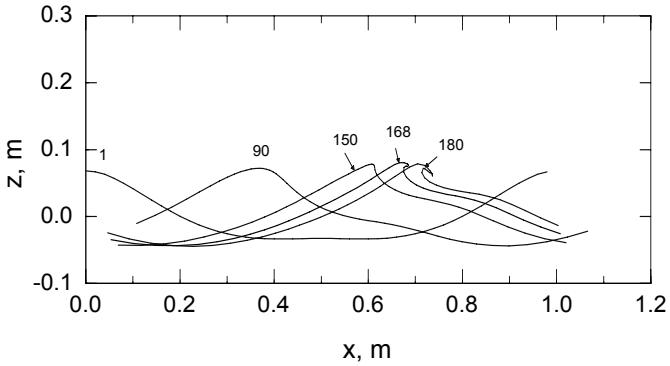

Figure 1. The evolution of a gravity wave.

III. Full-wave modeling of radar scattering

The starting point in our EM wave scattering simulation is a 2-D scalar Helmholtz equation with impedance (Leontovich) boundary conditions. This problem can be reduced to the solution of the following integral equation with respect to the surface value of the total field $\Psi(s)$ [8]:

$$\frac{1}{2}\Psi(\vec{r}) + \int \Psi(\vec{r}')\left(\frac{\partial}{\partial \vec{n}_{\vec{r}'}} + iKZ\right)\left(-\frac{i}{4}H_0^{(1)}\left(K|\vec{r}-\vec{r}'|\right)\right)d\Sigma_{\vec{r}'} = \Psi_{in}(\vec{r}). \quad (1)$$

Here, $k_0 = K\sin\theta_0$, $q_0 = K\cos\theta_0$ are horizontal and vertical components of the wave vector of the incident wave. For the case of vertical polarization, $Z = 1/\sqrt{\varepsilon}$, where ε is the dielectric constant of the scattered medium, and in this case, Z has the meaning of surface impedance. For the case of horizontal polarization $Z = \sqrt{\varepsilon}$. Note, that the impedance boundary condition is valid for $\varepsilon >> \max(1, \lambda / r_c)$, where r_c is the curvature radius of the surface.

By extracting the phase factor associated with the incident wave from the surface field, we introduce a new unknown function [8]:

$$\tilde{\Psi}(s) = \Psi(s)\exp\left[-ik_0 x(s) + iq_0 z(s)\right]. \quad (2)$$

In terms of $\tilde{\Psi}$, after simple transformations (1) becomes as follows:

$$\tilde{\Psi}(s) + \frac{1}{2}\int \tilde{\Psi}(s')\left[iKH_1^{(1)}\left(K|\vec{r}-\vec{r}'|\right)\frac{\frac{dx'}{ds'}(z'-z) - \frac{dz'}{ds'}(x'-x)}{|\vec{r}-\vec{r}'|} + \right. \quad (3)$$

$$\left. + KZH_0^{(1)}\left(K|\vec{r}-\vec{r}'|\right)\right]\exp\left[k_0(x'-x) - iq_0(z'-z)\right]ds' = 2\,.$$

This equation is solved numerically for the case of a periodic surface. In this case the scattered field consists of discrete spectra:

$$\Psi_{sc} = \sum_n S_n \exp(ik_n x - iq_n z), \quad (4)$$

where $k_n = k_0 + 2\pi n / L$, $q_n = \sqrt{K^2 - k_n^2}$, and L is the period of the surface. The amplitudes of spectra S_n can be expressed in terms of the surface field. Details of the full-wave EM code and its performance can be found in [4, 5].

IV. Ray-tracing modeling of radar scattering

To model radar scattering in the geometric optics approximation, we employ a ray-tracing approach. The ray-tracing algorithm works as follows: given a beam of parallel rays impinging onto a reflecting surface at an arbitrary incident angle, one finds ray intersections with the surface, then calculates reflected rays according to geometric optics laws, propagates them until they intersect the surface again, or intersect a receiving plane placed at some distance from the surface. This procedure is repeated for all rays until each of them arrives at the receiving plane. An example of such a simulation for the profile of a breaking wave is shown in Figure 2. Ray tracing gives a general picture of the scattering, demonstrates acts of multiple reflection, focusing, and caustics, but does not produce any amplitude characteristics. In order to calculate the amplitude associated with each ray, one needs to collect all the rays that arrive at a given receiving point, compute a change in a ray tube cross section that leads to an amplitude change, compute total phase along the ray including a phase shift due to caustics, and calculate a sum of the complex amplitudes for all rays. Note that both the amplitude and phase of the wave change upon reflection according to the polarization-sensitive Fresnel coefficient.

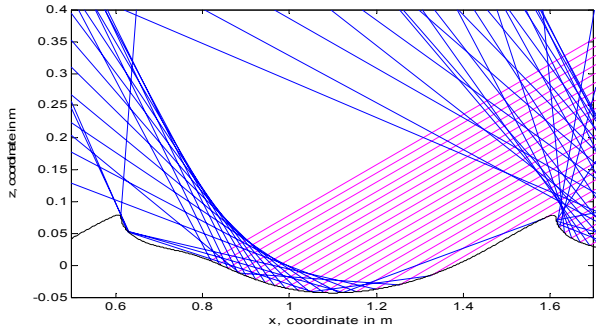

Figure 2. An example of ray-tracing simulations.

The output is a real and imaginary part of the scattered field (or a corresponding power) as a function of the x-coordinate in the receiving plane:

$$U(x) = |A_0| \left| \frac{dx_0}{dx} \frac{\cos\theta_0}{\cos\theta} \right|^{1/2} R_1 R_2 \ldots R_{N_f} \exp\left(-\frac{i\pi}{2} N_c + i \frac{\omega}{c} \sum_{j=1}^{N_r} |r_{j-1} - r_j| \right). \quad (5)$$

Here, U is the complex ray amplitude of the scattered field in the receiving point; A_0 is the initial ray amplitude; x_0 is the initial coordinate of the ray, x is the final coordinate of the ray; θ_0 is the angle of initial direction of the ray, θ is the angle of final direction of the ray; R_j is the Fresnel polarization-sensitive reflection coefficient at the j-th reflection from the surface; N_c is the number of points of the ray in which it is tangent with a caustic; and r_j is the coordinate of the ray at the j-th reflection. An example of ray and full-wave amplitude calculations for normal incidence onto the surface modeled by function $a\cos(2\pi x/\Lambda)$ (for λ = 2 cm, a = 2 cm, Λ = 6.28 m) is shown in Figures 3 and 4. The field is received at a horizontal plane z_r = 100 m.

Finally, angular power spectra for the scattered EM wave using the ray approach were calculated and compared with results from the full-wave approach (see Figures 5-11). Simulations were performed with an impedance that corresponds to dielectric constant ε = 54.3+i42.2 for sea water at 0°C and 35 ppm salinity for wavelength of 4.65 cm.

In Figures 5 and 6 a comparison between full-wave and ray-based calculations for angular spectra at HH- and VV-polarization at λ = 4.65 cm is presented for the case of both

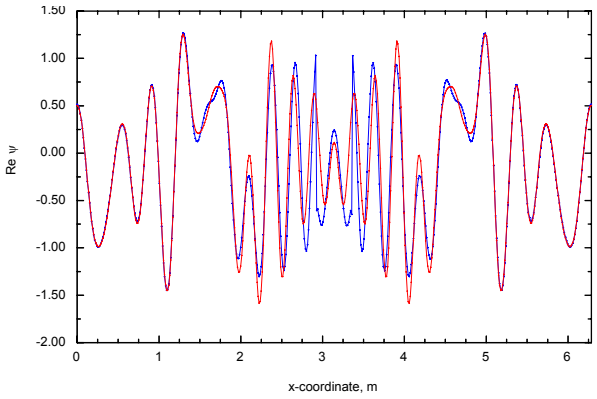

Figure 3. Real part of the scattered field at z_r = 100 m. The red curve depicts the full-wave solution, and the blue curve shows the ray solution.

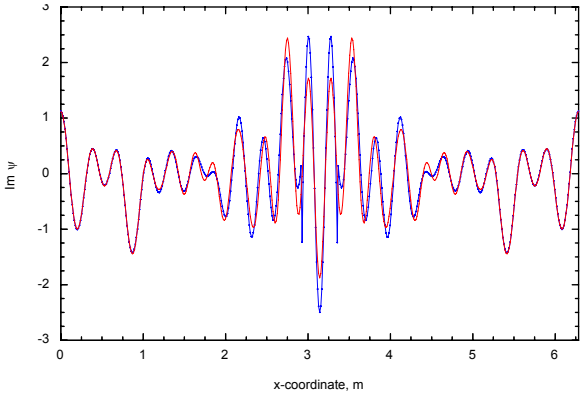

Figure 4. Imaginary part of the scattered field at z_r = 100 m. The red curve depicts the full-wave solution, and the blue curve shows the ray solution.

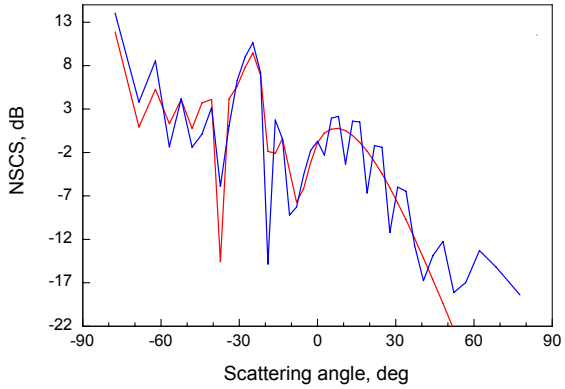

Figure 5. Angular spectrum at HH-polarization for 44 deg incident angle and for surface profile # 90 (see Figure 1).

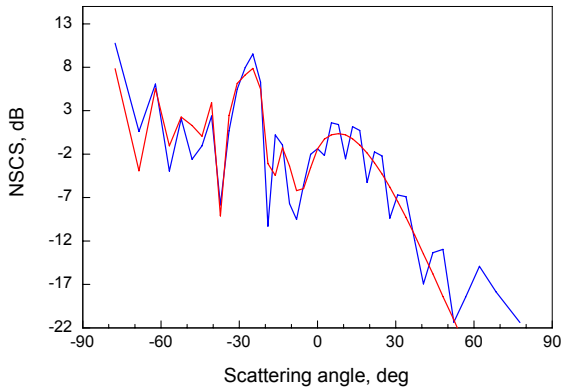

Figure 6. Angular spectrum at VV-polarization for 44 deg incident angle and for surface profile # 90.

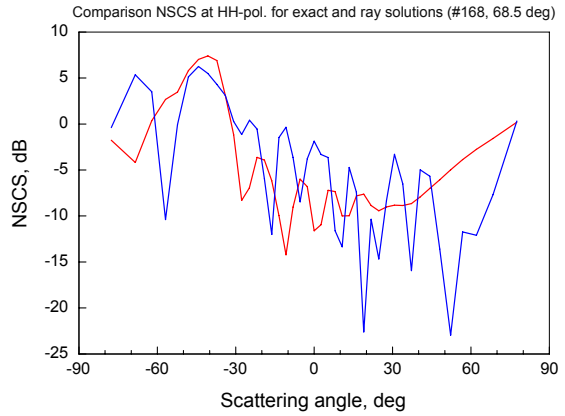

Figure 7. Angular spectrum at HH-polarization for 68 deg incident angle and for surface profile # 168.

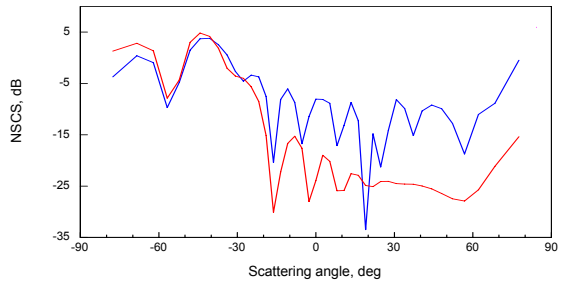

Figure 8. Angular spectrum at VV-polarization for 68 deg incident angle and for surface profile # 168.

moderate incidence and surface steepness. In Figures 7 and 8 analogous plots are shown for the case of greater grazing incidence and the breaking wave profile.

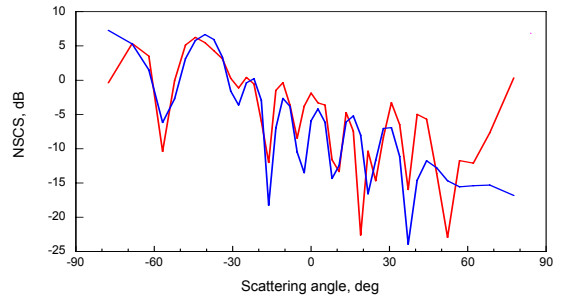

Figure 9. Angular spectrum at HH-polarization for 68 deg incidence and for profile # 168 based on a single reflection order (blue) and on all orders (red).

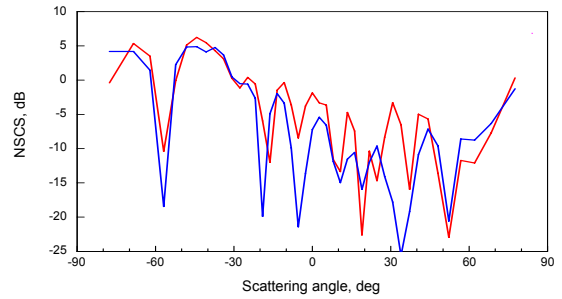

Figure 10. Angular spectrum at HH-pol. for 68 deg incidence and for profile # 168 based on three reflection orders (blue) and on all orders (red).

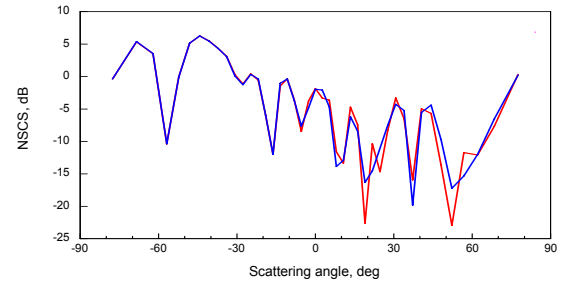

Figure 11. Angular spectrum at HH-polarization for 68 deg incidence and for profile # 168 based on five reflection orders (blue) and on all orders (red).

Figures 9-11 demonstrate results of ray simulations for angular spectra at HH-polarization accounting for rays with a different number (order) of reflections from the surface. Analogous results for VV-polarization (not shown here) demonstrate a better convergence over orders of reflections.

V. Discussion of Results

Comparison between angular power spectra obtained using the full-wave and the ray simulation demonstrates a better agreement for smoother surfaces and steeper incidence. For a given type of surface profile, better agreement is obtained for the forward-scattering directions than for the backscattering directions. Ray simulation for the backscattering direction does not reproduce the HH/VV ratio observed in the full-wave solution. This indicates that simplistic geometric optics models for backscattering from breaking waves are not satisfactory, and that diffraction effects are critical for explaining important features of backscattering from breaking waves. Figures 9-11 show that forward scattering is determined mainly by first orders of reflections. In the case of VV polarization, even a single reflection contributes the most in the forward direction, whereas for HH-polarization it requires up to five orders of reflections to approach the saturation. It is evident that more than 5 orders are needed to describe scattering in non-specular directions (between -20 and 50 deg). It is also important to note that due to relatively steep profile slopes, maxima of forward scattering occur at smaller scattering angles rather than along the direction of the nominal specular reflection from the average plane.

The role of multiple reflections from a breaking wave profile in creating spikes in a backscattering direction with an anomalous HH/VV ratio proves to be negligible.

References

[1] A.G. Voronovich and V.U. Zavorotny, "Theoretical model for scattering of radar signals in K_u- and C-bands from a rough sea surface with breaking waves," *Waves Random Media*, vol. 11, pp. 247–269, 2001.

[2] J.C. West, J.M. Sturm, and S.-J. Ja, "Low-grazing scattering from breaking water waves using an impedance boundary MM/GTD approach," *IEEE Trans. Antennas Propagat*., vol. 46, pp. 93–100, 1998.

[3] D. Holliday, L.L. DeRaad, Jr., and G. J. St.- Cyr, "Sea-spike backscatter from a steepening wave," *IEEE Trans. Antennas Propagat*., vol. 46, pp. 108–113, 1998.

[4] A.G. Voronovich and V.U. Zavorotny, "Scattering of electromagnetic waves from breaking surface gravity waves," *Proc. Int. Conf. Electromagnetics in Advanced Applications (ICEAA'05)*, Torino, Italy, 2005.

[5] A.G. Voronovich and V.U. Zavorotny, "A numerical model of radar scattering from steep and breaking waves," *Proc. Int. Geosci. Remote Sens. Symp. (IGARSS'06)*, Denver, Colorado, 2006.

[6] A.T. Jessup, W.C. Keller, and W.K. Melville, "Measurements of sea spikes in microwave backscatter at moderate incidence," *J. Geophys. Res*., vol. 95, pp. 9679–9688, 1990.

[7] Y. Liu, S.J. Frasier, and R.E. Mcintosh, "Measurement and classification of low-grazing-angle radar sea spikes," *IEEE Trans. Antennas Propagat*. , vol. 46, pp. 27–40, 1998.

[8] A.G. Voronovich and V.U. Zavorotny, "The effect of steep sea-waves on polarization ratio at low grazing angles," *IEEE Trans. Geosci. Remote Sensing*, vol. 38, pp. 366–373, 2000.